ASTROBIOLOGY
Volume 22, Number 2, 2022
Mary Ann Liebert, Inc.
DOI: 10.1089/ast.2021.0012

Research Articles

Nitrogen Cycling and Biosignatures in a Hyperarid Mars Analog Environment

Jianxun Shen,[i] Aubrey L. Zerkle,[ii] and Mark W. Claire[iii]

Abstract

The hyperarid Atacama Desert is a unique Mars-analog environment with a large near-surface soil nitrate reservoir due to the lack of rainfall leaching for millennia. We investigated nitrogen (N) cycling and organic matter dynamics in this nitrate-rich terrestrial environment by analyzing the concentrations and isotopic compositions of nitrate, organic C, and organic N, coupled with microbial pathway-enzyme inferences, across a naturally occurring rainfall gradient. Nitrate deposits in sites with an annual precipitation of <10 mm carry atmospheric $\delta^{15}N$, $\delta^{18}O$, and $\Delta^{17}O$ signatures, while these values are overprinted by biological cycling in sites with >15 mm annual precipitation. Metagenomic analyses suggest that the Atacama Desert harbors a unique biological nitrogen cycle driven by nitrifier denitrification, nitric oxide dioxygenase-driven alternative nitrification, and organic N loss pathways. Nitrate assimilation is the only nitrate consumption pathway available in the driest sites, although some hyperarid sites also support organisms with ammonia lyase- and nitric oxide synthase-driven organic N loss. Nitrifier denitrification is enhanced in the ''transition zone'' desert environments, which are generally hyperarid but see occasional large rainfall events, and shifts to nitric oxide dioxygenase-driven alternative nitrifications in wetter arid sites. Since extremophilic microorganisms tend to exploit all reachable nutrients, both N and O isotope fractionations during N transformations are reduced. These results suggest that N cycling on the more recent dry Mars might be dominated by nitrate assimilation that cycles atmospheric nitrate and exchanges water O during intermittent wetting, resulting stable isotope biosignatures could shift away from martian atmospheric nitrate endmember. Early wetter Mars could nurture putative life that metabolized nitrate with traceable paleoenvironmental isotopic markers similar to microbial denitrification and nitrification stored in deep subsurface. Key Words: Nitrate stable isotopes—Organic isotopes—Enzyme pathway inferences—N cycling—Models. Astrobiology 22, 127–142.

1. Introduction

The central depression of the Atacama Desert in northern Chile is embedded between the Coastal Range and the Andes mountains, and has been extremely dry for more than 10 million years due to amplification of local climatic effects by the Andean uplift (Rech *et al.*, 2006; Sun *et al.*, 2018). The altitudes of the Coastal Range (*Cordillera de la Costa*) and the Andes are generally between 2000 and 6000 m, while the altitude of the central Atacama is about 900–2500 m (Sernageomin, 2003). Soil temperatures in the dry areas of the Atacama Desert varied from −4.9°C to 57.4°C between the years 1994 to 1998, and the soil relative humidity can vary from 9% to 64%.

Because of the intense ionizing radiation and ultraviolet (UV)-driven photochemical reactions, the Atacama Desert acts as a perfect model to study natural salt deposits derived from the atmosphere (Melchiorre *et al.*, 2018; Xu *et al.*, 2019). Large reservoirs of multiple oxyanions, including nitrate, sulfate, perchlorate, manganese oxides, and iron oxides, have developed in this region (Michalski *et al.*, 2004; Fernandez-Remolar *et al.*, 2013; Xu *et al.*, 2019). The Atacama Desert is one of the nonpolar deserts that contain a huge nitrate reservoir, and the near-surface presence of nitrate has been exploited for hundreds of years.

Nitrate salts are highly soluble and generally leached from most soil profiles, but the miniscule rainfall in hyperarid regions permits its accumulation in the shallow

School of Earth and Environmental Sciences and Centre for Exoplanet Science, University of St Andrews, St Andrews, United Kingdom.
[i]ORCID ID (https://orcid.org/0000-0002-3942-1692).
[ii]ORCID ID (https://orcid.org/0000-0003-2324-1619).
[iii]ORCID ID (https://orcid.org/0000-0001-9518-089X).

subsurface (Walvoord *et al.*, 2003), and nitrates become one of the important constituents of Atacama mineralogy. The common nitrate minerals include Chilean saltpeter $NaNO_3$, darapskite $Na_3(SO_4)(NO_3)\cdot H_2O$, and humberstonite $Na_7K_3Mg_2(SO_4)_6(NO_3)_2\cdot 6H_2O$ (Ericksen, 1983). Similarly, nitrate deposits in martian sediments ranging from 70 to 1100 parts per million (ppm), as determined at the Gale Crater and in martian meteorites (Kounaves *et al.*, 2014; Stern *et al.*, 2015; Jaramillo *et al.*, 2019), are assumed to derive from atmospheric photochemistry (Michalski *et al.*, 2004; Catling *et al.*, 2010; Smith *et al.*, 2014). Thus, the hyperarid core of the Atacama Desert has long been considered an analog for Amazonian Mars, due to its large nitrate reservoirs, hyperarid conditions, and high UV intensities (*e.g.*, Navarro-Gonzalez *et al.*, 2003; Shen *et al.*, 2019).

Due to its overwhelming abundance over other nitrogen (N) sources, nitrate likely drives biological N cycling in hyperarid soils (Shen *et al.*, 2019). Stable N and oxygen (O) isotopes of nitrate have long been utilized as useful tools to unravel the environmental N sources and cycling processes. As microorganisms consume or produce nitrate, the isotopes of N and O are fractionated by these biological transformations in accordance with the priority of lighter isotopes (Casciotti *et al.*, 2013). O isotopes are also affected by the O atom sources incorporated into nitrate, such as water and atmospheric O_2 (Buchwald and Casciotti, 2010; Casciotti *et al.*, 2010). Worldwide, desert soils contain intriguing correlations between N/O isotopes and indicators of water/microbial activity (Jackson *et al.*, 2015), which motivated some of the work presented here.

With enhanced microbial N cycling in the soils, the N and O isotope ratios of an abiotic atmospheric nitrate source can be overprinted and preserved as a biosignature. N cycling is one of the key components of biogeochemical ecosystem functioning because of the fundamental roles of N in all organisms. Nitrate can be biologically cycled directly by processes such as denitrification, dissimilatory nitrate reduction to ammonium (DNRA or nitrate ammonification), and assimilatory nitrate reduction (or nitrate assimilation). Denitrification and DNRA are the processes that reduce nitrate to N_2 and ammonium (NH_4^+), respectively, with nitrite (NO_2^-) as an intermediate product (Lam and Kuypers, 2011). Assimilatory nitrate reduction is the process of microbial assimilation of nitrate for the incorporation into organonitrogen compounds (Wada and Hattori, 1978; Tischner, 2000). These three processes all require nitrate molecules to pass through cell membranes and enter the outer or inner bacterial membranes or periplasm for reductive catalysis (Granger *et al.*, 2004, 2008). All of these N cycling pathways are catalyzed by enzymes (Montoya, 2008; Casciotti, 2009), which impart distinctive isotopic partitioning.

These biological N cycling processes generally result in kinetic fractionation of N and O isotopes that can be expressed in the residual nitrate or organic N products. The ranges of isotopic enrichment factors of denitrification, DNRA, assimilatory nitrate reduction, and nitrification are illustrated in Fig. 1. In nitrate reduction and assimilation, the enrichment factor of O is usually very close to the factor of N (Sigman *et al.*, 2005; Granger *et al.*, 2010). These fractionation effects can vary significantly, for example, depending on microbial growth rate and nitrate concentrations (Kohl and Shearer, 1980; Mariotti *et al.*, 1980, 1982).

Since Atacama nitrate deposits are derived from the atmosphere, their $\delta^{15}N$, $\delta^{18}O$, and $\Delta^{17}O$ values (as defined in the Materials and Methods section) should primarily reflect their sources, which are ultimately dinitrogen gas (N_2) and some mixture of ozone (O_3), oxygen (O_2), and OH derived from H_2O, respectively (Reich and Bao, 2018). Atmospheric N_2 has a $\delta^{15}N$ value of 0‰ by definition, and most (pollution-free) NO_x species also feature a $\delta^{15}N$ close to zero. Broadly speaking, the O atoms in atmospheric nitrate are a mixture (Michalski *et al.*, 2003, 2014) from O_3 (with $\Delta^{17}O$ of transferrable O up to 39‰ and $\delta^{18}O$ of O_3 as high as 115‰—[Vicars and Savarino, 2014]) and from atmospheric water with $\Delta^{17}O$ and variable $\delta^{18}O$ (Fig. 1).

Previous studies have measured $\delta^{15}N_{NO3}$ values in Atacama nitrates ranging from −5‰ to +8‰ (Bohlke *et al.*, 1997; Michalski *et al.*, 2004; Ewing *et al.*, 2007; Melchiorre *et al.*, 2018). Compared with more biologically active environments (Qin *et al.*, 2012), $\delta^{15}N$ values in Atacama nitrate are generally low, implying that the extent of microbial nitrate reduction is insufficient to overprint the atmospheric isotope signatures. Previously measured $\delta^{18}O_{NO3}$ values from Atacama nitrates vary from 31‰ to 64‰ (Michalski *et al.*, 2004; Ewing *et al.*, 2007), similar to other sites that preserve large atmospheric nitrate deposits (Michalski *et al.*, 2005; Qin *et al.*, 2012). The $\Delta^{17}O_{NO3}$ of Atacama nitrate can be as high as 9‰ to 23‰ (Michalski *et al.*, 2004; Ewing *et al.*, 2007). Since biological processes follow mass-dependent fractionation, the biological signal of $\Delta^{17}O_{NO3}$ is approximately zero. Thus, these high $\Delta^{17}O_{NO3}$ values demonstrate the atmospheric origin of nitrate deposits in the Atacama Desert.

Cross-plots of $\delta^{15}N_{NO3}$ versus $\delta^{18}O_{NO3}$ from the Atacama and other more humid deserts suggest a distinct abiotic atmospheric endmember nitrate composition that takes on differential isotopic signatures after biological processing (Jackson *et al.*, 2015). If better understood, N/O isotope systematics in nitrate could function as a geochemical biosignature that could be explored robotically on Mars or on returned samples. During microbial nitrate consumptions, fractionations in $\delta^{18}O_{NO3}$ largely reflect the $\delta^{18}O$ values of O in ambient water absorbed by microorganisms (Casciotti 2009). However, the relevant N and O isotope fractionation effects have largely been measured in laboratory enrichment cultures and in water-rich or aqueous environments, which may not express in the extremely dry condition as the Atacama Desert, or indeed, Mars itself.

Here we examine the stable isotope variations in nitrates ($\delta^{15}N$, $\delta^{18}O$, and $\Delta^{17}O$) along an aridity gradient in the Atacama Desert, to determine when and how biological N cycling acts to modify atmospheric N and O isotope signals in a dry Mars analog environment. We combine these analyses with $\delta^{15}N$ and carbon isotope ($\delta^{13}C$) analyses, soil metagenome extraction, and microbial pathway-enzyme inferences in associated organic matter to directly match the resulting N isotope biosignatures to the microbial processes they represent. This study contributes to quantifying potential isotopic fractionation

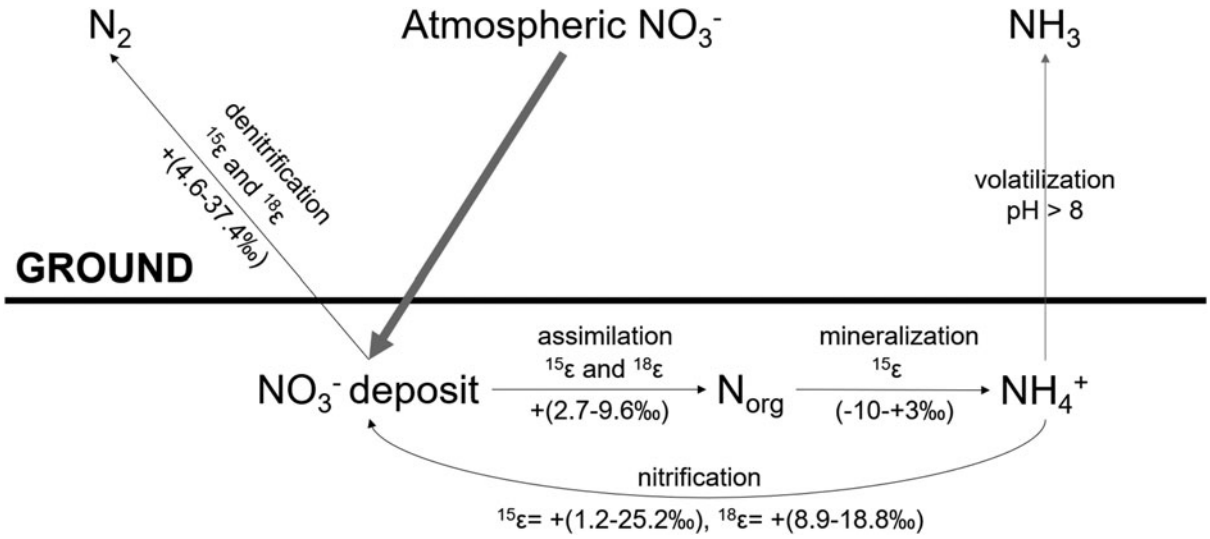

FIG. 1. Schematic diagram of a hypothesized N cycle for a hyperarid environment, including deposition of nitrate, denitrification (includes DNRA range), assimilatory nitrate reduction, mineralization, and nitrification, illustrating the ranges of N and O isotopic enrichment factors (Mccready *et al.*, 1983; Bottcher *et al.*, 1990; Casciotti, 2009; Sigman *et al.*, 2009; Vicars and Savarino, 2014; Granger and Wankel, 2016; Stueken *et al.*, 2016; Denk *et al.*, 2017). ε is defined by $\delta_{reactant}-\delta_{product}$. Black arrows denote biological processes; red arrows denote abiotic processes. DNRA = dissimilatory nitrate reduction to ammonium.

effects and resulting biosignatures of N transformation processes in a hyperarid Mars-analogous landscape, with a focus on identifying geochemical biosignatures measurable by robotic exploration.

2. Materials and Methods

2.1. Geochemical characterization and statistical analyses

The detailed descriptions of study sites, sampling, and geochemical analytical methods are reported in the work of Shen *et al.* (2019). Briefly, samples from ~15 cm depth were taken in triplicate from seven sites at roughly 1143 ± 392 m elevation in the central depression of the Atacama Desert, along a latitudinal gradient that reflects increasing annual rainfall (Fig. 2). From the driest north to the wettest south, these sites were María Elena South (MES), Point of No Return (PONR), Yungay, Transition Zone (TZ) TZ-0, TZ-4, TZ-5, and TZ-6. Based on hierarchical cluster analysis of measured geophysical and geochemical values, MES, PONR, Yungay, and TZ-0 were designated as hyperarid sites; TZ-4 was designated as a transitional site; TZ-5 and TZ-6 were designated as arid sites (Shen *et al.*, 2019). The annual precipitation of each sampling site was calculated as the mean value of multiple nearest rain gauges between 1951 and 2017 (the sampling year) from Explorador Climático, Center for Climate and Resilience Research (Shen *et al.*, 2019).

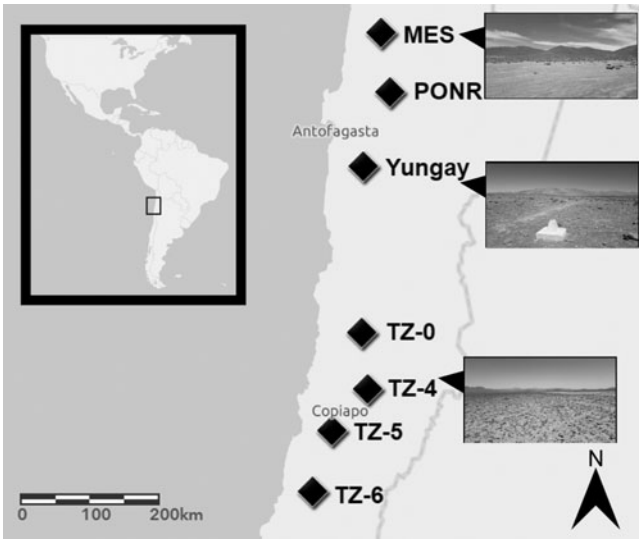

FIG. 2. Sampling sites in the Atacama Desert, Northern Chile.

Concentrations of nitrate, NO_2^-, and ammonium were measured in triplicate by ion chromatography (IC) at the University of St Andrews and using standard methods detailed in the work of Shen *et al.* (2019). Soils were pulverized and decarbonated by using dilute (10% HCl) for total organic C (TOC), total N (TN), and C and N isotope ratios, and they were analyzed by elemental analysis/isotope ratio mass spectrometry at the University of St Andrews (Stueken *et al.*, 2017; Shen *et al.*, 2019). Since the concentrations of TN were significantly correlated with those of TOC, the ammonium concentrations were minimal, and TN did not exhibit correlation with the clay-bound potassium (determined by X-ray fluorescence), the TN contents were referred to as the total organic N (TON), and N isotope values were referred to as $\delta^{15}N_{org}$ (as reported in Shen *et al.*, 2019). Carbon and nitrogen isotopes were calibrated with USGS-40, USGS-41, USGS-62, and SGR-1b. USGS-62 (with $\delta^{13}C$ of −14.79‰ and $\delta^{15}N$ of 20.17‰) was measured as samples for quality control, which returned experimental $\delta^{13}C$ values of −14.89 ± 0.19‰ and $\delta^{15}N$ values of 19.83 ± 0.36‰.

We additionally performed normality test and bivariate correlation analyses on geochemical data using IBM SPSS

Statistics 26 (IBM Corp, 2019). If both variables were normally distributed, Pearson's r correlation was used. Otherwise, Spearman's ρ correlation was used.

2.2. Bacterial denitrifier and thermal decomposition methods

Soil NO_3^- (plus trivial NO_2^-) used for isotope analyses were re-extracted and quantified by using IC, and they were kept at −20°C. Stable isotopes ($\delta^{18}O$, $\Delta^{17}O$, and $\delta^{15}N$, as defined below) of the extracted NO_3^- were measured by the coupled bacterial denitrifier and thermal decomposition method described in the work of Kaiser *et al.* (2007) at the Science Analytical Facilities of the University of East Anglia. In brief, *Pseudomonas chlororaphis* spp. *aureofaciens*, a strain of denitrifying bacteria deficient in nitrous oxide (N_2O) reductase, was used to convert 50 nmol NO_3^- into N_2O (Sigman *et al.*, 2001; Casciotti *et al.*, 2002) that was then pyrolyzed to N_2 and O_2 by decomposition in a gold furnace at 800°C (Kaiser *et al.*, 2007). N_2 and O_2 were separated and analyzed on a Geo 20-20 device by gas chromatography-isotope ratio mass spectrometry (Comer-Warner *et al.*, 2020). International nitrate reference standards USGS-34, USGS-35, and IAEA-NO3 were used to calibrate the triple nitrate isotope measurements. The precisions for the $\delta^{18}O$, $\Delta^{17}O$, and $\delta^{15}N$ analyses were typically up to ±2.1‰, ±0.5‰, and ±0.2‰, respectively (1σ based on replicate standard measurements).

We herein define the δ and Δ isotope ratio notations as follows:

$$\delta^{15}\mathrm{N}\ (‰) = \left(\frac{{}^{15}_{0}\mathrm{R}_{\mathrm{sample}}}{{}^{15}_{0}\mathrm{R}_{\mathrm{standard}}} - 1\right) \times 1000 \quad (1)$$

$$\delta^{18}\mathrm{O}\ (‰) = \left(\frac{{}^{18}_{0}\mathrm{R}_{\mathrm{sample}}}{{}^{18}_{0}\mathrm{R}_{\mathrm{standard}}} - 1\right) \times 1000 \quad (2)$$

$$\delta^{17}\mathrm{O}\ (‰) = \left(\frac{{}^{17}_{0}\mathrm{R}_{\mathrm{sample}}}{{}^{17}_{0}\mathrm{R}_{\mathrm{standard}}} - 1\right) \times 1000 \quad (3)$$

$$\Delta^{17}\mathrm{O}\ (‰) = \left[\frac{\left(\frac{\delta^{17}\mathrm{O}}{1000} + 1\right)}{\left(\frac{\delta^{18}\mathrm{O}}{1000} + 1\right)^{0.528}} - 1\right] \times 1000 \quad (4)$$

where ${}^{xx}\mathrm{R}_{\mathrm{sample}}$ is the $^{15}N/^{14}N$, $^{18}O/^{16}O$, or $^{17}O/^{16}O$ ratio in a given sample, and ${}^{xx}\mathrm{R}_{\mathrm{standard}}$ is the corresponding ratio of international standards, that is, atmospheric N_2 for N stable isotopes and Vienna Standard Mean Ocean Water for O stable isotopes. We further define the isotopic enrichment factors, $^{15}\varepsilon$ and $^{18}\varepsilon$, as follows:

$${}^{15}_{0}\varepsilon\ (‰) \approx \delta^{15}\mathrm{N}_{\mathrm{reactant}} - \delta^{15}\mathrm{N}_{\mathrm{product}} \quad (5)$$

$${}^{18}_{0}\varepsilon\ (‰) \approx \delta^{18}\mathrm{O}_{\mathrm{reactant}} - \delta^{18}\mathrm{O}_{\mathrm{product}} \quad (6)$$

2.3. Enzyme and functional pathway inferences

The soil metagenome extraction, 16S rRNA gene sequencing, and enzyme and functional pathway inferences were described in detail in the works of Shen *et al.* (2020) and Shen *et al.* (2021). Briefly, only three sites of MES, two sites of TZ-0, three sites of TZ-4, three sites of TZ-5, and three sites of TZ-6 obtained sufficient yields for Illumina sequencing. 16S rRNA amplicons for Illumina MiSeq System were sequenced following the protocol *16S Metagenomic Sequencing Library Preparation* (Illumina® 2013). Potential functions of these sequences were inferred by PICRUSt2 (Douglas *et al.*, 2019) referencing the Enzyme Commission and MetaCyc pathway databases (Shen *et al.*, 2020, 2021). Here, we focus solely on enzymes and pathways that are relevant to N cycling, and these were converted to heatmaps with OriginPro 2019 (OriginLab Corp, 2019).

3. Results

3.1. Nitrate, nitrite, and ammonium

The concentrations of nitrate and TON were previously reported in the work of Shen *et al.* (2019) (Table 1 and Fig. 3a, b). In summary, nitrate and TON concentrations ranged 1.4–6800 ppm and 18–180 ppm, respectively. Hyperarid sites PONR and Yungay had the highest concentrations of NO_2^-, between 0.77 and 0.87 ppm (Table 1 and Fig. 3c). High NO_2^- was associated with the rainfall event in 2017. Other sites all had low NO_2^- concentrations from 0.001 to 0.11 ppm. Ammonium remained at low levels from 0.02 to 0.3 ppm and did not show a trend with either precipitation data (Fig. 3c).

3.2. C/N molar ratios, $\delta^{13}C_{org}$, and $\delta^{15}N_{org}$

The organic C/N molar ratios in the hyperarid (MES, PONR, Yungay, and TZ-0) and transitional (TZ-4) sites were between 1 and 4, while C/N ratios in the arid sites (TZ-5 and TZ-6) were between 8 and 11 (Table 1 and Fig. 4a). $\delta^{13}C_{org}$ ranged from −30‰ in the hyperarid sites to −21‰ in the arid sites. $\delta^{15}N_{org}$ ranged from +3‰ in the hyperarid sites to +11‰ in the arid sites. Both C and N isotope ratios were positively correlated with the concentrations of organic matter (Fig. 4b, d). Different C/N ratios were grouped with $\delta^{13}C_{org}$, and high C/N ratios were associated with C sources of high $\delta^{13}C_{org}$ (Fig. 4c). $\delta^{15}N_{org}$ values did not clearly associate with C/N ratios or $\delta^{13}C_{org}$ values but were more closely related to the aridity of sites (Fig. 4e, f).

3.3. Nitrate stable isotopes

NO_2^- constituted from 0.001% to 6% of the Atacama nitrate deposit and contributed minimally to the isotope values (Table 2). In the hyperarid sites, $\delta^{18}O_{NO3}$, $\Delta^{17}O_{NO3}$, and $\delta^{15}N_{NO3}$ ranged from +60‰ to +74‰, from +19‰ to +23‰, and from −3‰ to +2‰, respectively (Fig. 5a). In the transitional and arid sites, $\delta^{18}O_{NO3}$ and $\Delta^{17}O_{NO3}$ ranged from +17‰ to +40‰ and from +3‰ to +13‰, respectively. However, the $\delta^{15}N_{NO3}$ values of the transitional and arid sites were variable within these sites: the $\delta^{15}N_{NO3}$ of TZ-4 and TZ-6 ranged from +5‰ to +8‰, but the $\delta^{15}N_{NO3}$ of TZ-5 ranged from +1‰ to +3‰ (Table 2 and Fig. 5a). As $\delta^{15}N_{NO3}$ increased, $\delta^{18}O_{NO3}$ and $\Delta^{17}O_{NO3}$ dropped from the hyperarid to the transitional and arid sites (Fig. 5b). $\delta^{18}O_{NO3}$ and $\Delta^{17}O_{NO3}$ were positively associated with each other (Fig. 5c). According to correlation analyses, $\delta^{15}N_{NO3}$ was significantly positively correlated with $\delta^{15}N_{org}$ ($\rho = 0.75$***, $p < 0.001$), $\delta^{13}C_{org}$ ($\rho = 0.67$***, $p < 0.001$), TON ($\rho = 0.67$***, $p < 0.001$), and TOC ($\rho = 0.57$**, $p = 0.003$) (Fig. 5d–f).

Table 1. Concentrations of Nitrate (from Shen *et al.*, 2019), Nitrite, and Ammonium, Molar Ratios of Organic C to N, and Stable Isotope Ratios of Organic C and N (Mean ± Standard Errors on Triplicates When Applicable)

Site	NO_3^- *(ppm)*	NO_2^- *(ppb)*	NH_4^+ *(ppb)*	C_{org}/N_{org} *(mol/mol)*	$\delta^{13}C_{org}$ (‰)	$\delta^{15}N_{org}$ (‰)
M1	35.7 ± 0.3	95.0 ± 29.4	—	3.18	−26.34 ± 0.45	4.79 ± 0.73
M2	238.4 ± 3.6	66.3 ± 27.4	—	2.12	−27.25 ± 0.23	5.30 ± 0.47
M3	52.1 ± 0.2	87.0 ± 32.2	37.0 ± 9.3	2.27	−27.44 ± 0.21	4.63 ± 0.38
P1	147.5 ± 2.5	839.3 ± 305.9	—	2.08	−26.46 ± 0.08	5.18 ± 0.27
P2	362.0 ± 39.1	766.3 ± 318.8	—	1.27	−26.28 ± 0.08	6.47 ± 0.04
P3	157.7 ± 2.6	837.7 ± 254.1	193.3 ± 7.3	2.60	−26.49 ± 0.20	5.47 ± 0.50
Y1	23.8 ± 0.1	790.7 ± 254.8	—	1.98	−27.30 ± 0.12	3.70 ± 0.31
Y2	19.3 ± 1.0	870.0 ± 286.9	—	2.30	−26.75 ± 0.29	3.87 ± 0.34
Y3	15.5 ± 0.3	872.0 ± 276.0	190.7 ± 33.8	2.15	−26.79 ± 0.32	4.12 ± 0.21
T01	1.9 ± 0.0	91.0 ± 29.4	—	3.63	−29.05 ± 0.47	4.86 ± 0.10
T02	1.4 ± 0.0	81.0 ± 25.1	—	3.18	−28.18 ± 0.12	5.67 ± 0.07
T03	2.5 ± 0.0	86.7 ± 27.6	157.3 ± 6.1	3.47	−29.15 ± 0.03	7.05 ± 0.35
T41	2686.8 ± 141.6	43.0 ± 15.7	20.7 ± 1.9	3.06	−25.58 ± 0.23	9.80 ± 0.12
T42	6802.6 ± 290.2	113.0 ± 50.0	—	2.73	−27.04 ± 0.37	9.74 ± 0.02
T43	4100.0 ± 160.4	56.0 ± 20.8	—	2.57	−26.33 ± 0.04	9.40 ± 0.10
T51	3.0 ± 0.1	30.7 ± 21.7	297.0 ± 25.1	9.97	−23.78 ± 0.00	7.32 ± 0.14
T52	6.0 ± 0.1	0.7 ± 0.3	—	9.96	−22.49 ± 0.02	7.23 ± 0.14
T53	20.9 ± 0.2	42.0 ± 4.0	—	10.87	−21.76 ± 0.01	7.94 ± 0.07
T61	11.7 ± 0.2	74.7 ± 30.7	77.7 ± 33.5	8.71	−22.98 ± 0.02	8.82 ± 0.06
T62	140.6 ± 1.3	13.7 ± 0.3	—	10.40	−22.83 ± 0.10	8.14 ± 0.08
T63	82.4 ± 0.8	1.3 ± 1.3	—	9.45	−22.62 ± 0.01	10.87 ± 0.09

M1–M3, three MES pits; P1-P3, three PONR pits; Y1–Y3, three Yungay pits; T01–T03, three TZ-0 pits; T41–T43, three TZ-4 pits; T51–T53, three TZ-5 pits; T61–T63, three TZ-6 pits.
— = not measured; MES = María Elena South; NH_4^+ = ammonium; NO_2^- = nitrite; PONR = Point of No Return; TZ = Transition Zone.

3.4. N cycling enzymes and pathways

Pathway inference results of 16S rRNA gene sequencing demonstrate that the only full pathways of N cycling-related metabolisms were assimilatory nitrate reduction (nitrate assimilation), denitrification, and nitrifier denitrification (Fig. 6), and that related enzymes included nitrogenase, NO_2^- reductases, nitrate reductases, N_2O reductase, nitric oxide reductase, dioxygenase, synthase, hydroxylamine reductase and dehydrogenase, and ammonia monooxygenase, lyases, and ligases (Fig. 7 and Table 3).

Assimilatory nitrate reduction was consistently the most abundant N metabolism in all sites (Fig. 6). Denitrification also universally existed in all sites but at slightly lower abundances in the hyperarid site MES. Nitrifier denitrification was significantly more dominant in TZ-0 than other sites, and TZ-0 was the only site that had more abundant nitrifier denitrification pathways than the normal denitrification pathways.

The universally abundant N enzymes were glutamate-ammonia ligase, adenylyltransferase, threonine ammonia-lyase, histidine ammonia-lyase, L-serine ammonia-lyase, nitrate reductase, and NO_2^- reductase (Fig. 7). Ammonia monooxygenase and hydroxylamine dehydrogenase were not predicted in MES. The transitional and arid sites had more dominant nitric oxide synthase and dioxygenase than the hyperarid sites (Table 3).

4. Discussion

4.1. Atmospheric and biological signatures in Atacama nitrate deposits

Nitrate in the hyperarid sites had high $\delta^{18}O$ and $\Delta^{17}O$ and near-0‰ $\delta^{15}N$ values (Table 2 and Fig. 5a), suggesting a predominantly atmospheric source (Ewing *et al.*, 2007; Melchiorre and Talyn, 2014; Reich and Bao, 2018). NO_2^- composed <6% of total nitrate deposits (Table 2), and transformations between NO_2^- and nitrate did not seem to produce a significant fractionation effect, since $\delta^{15}N_{NO3}$ values were not correlated with NO_2^- concentrations (Supplementary Fig. S1b). In transitional and arid sites, biological activity mostly overprinted the atmospheric stable isotope signals in the nitrate (Fig. 5b), although an atmospherically derived correlation between $\delta^{18}O_{NO3}$ and $\Delta^{17}O_{NO3}$ still exists (Fig. 5c).

Based on mass balance calculations assuming the $\Delta^{17}O_{NO3}$ value of 22.9‰ for atmospheric nitrate, 95 ± 4% of the total nitrate deposit in hyperarid sites was atmospherically derived, while 34 ± 10% of the nitrate was atmospheric in the transitional and arid sites (Table 2). This suggests that up to 60% of nitrate in the transitional and arid sites was derived from biological exchange (*i.e.*, from microbial nitrification, denitrification, and assimilation) between intermediate nitrogen oxide species and surrounding water molecules (Casciotti, 2009). Microbial activity tends to decrease the values of $\delta^{18}O_{NO3}$, because the local water sources for Atacama microbial communities are mostly ^{18}O-depleted snowmelt and rainwater (Fritz *et al.*, 1981; Schotterer *et al.*, 1996; Aravena *et al.*, 1999; Boschetti *et al.*, 2019; Jordan *et al.*, 2019).

Denitrification and nitrate assimilation likely contributed to the modification of residual nitrate deposits when the intermediate product NO_2^- was kinetically converted back to nitrate (Casciotti, 2009; Reich and Bao, 2018). Since denitrification transforms lighter N isotopes from solid to gaseous phase, the $\delta^{15}N$ of leftover nitrate pool remains

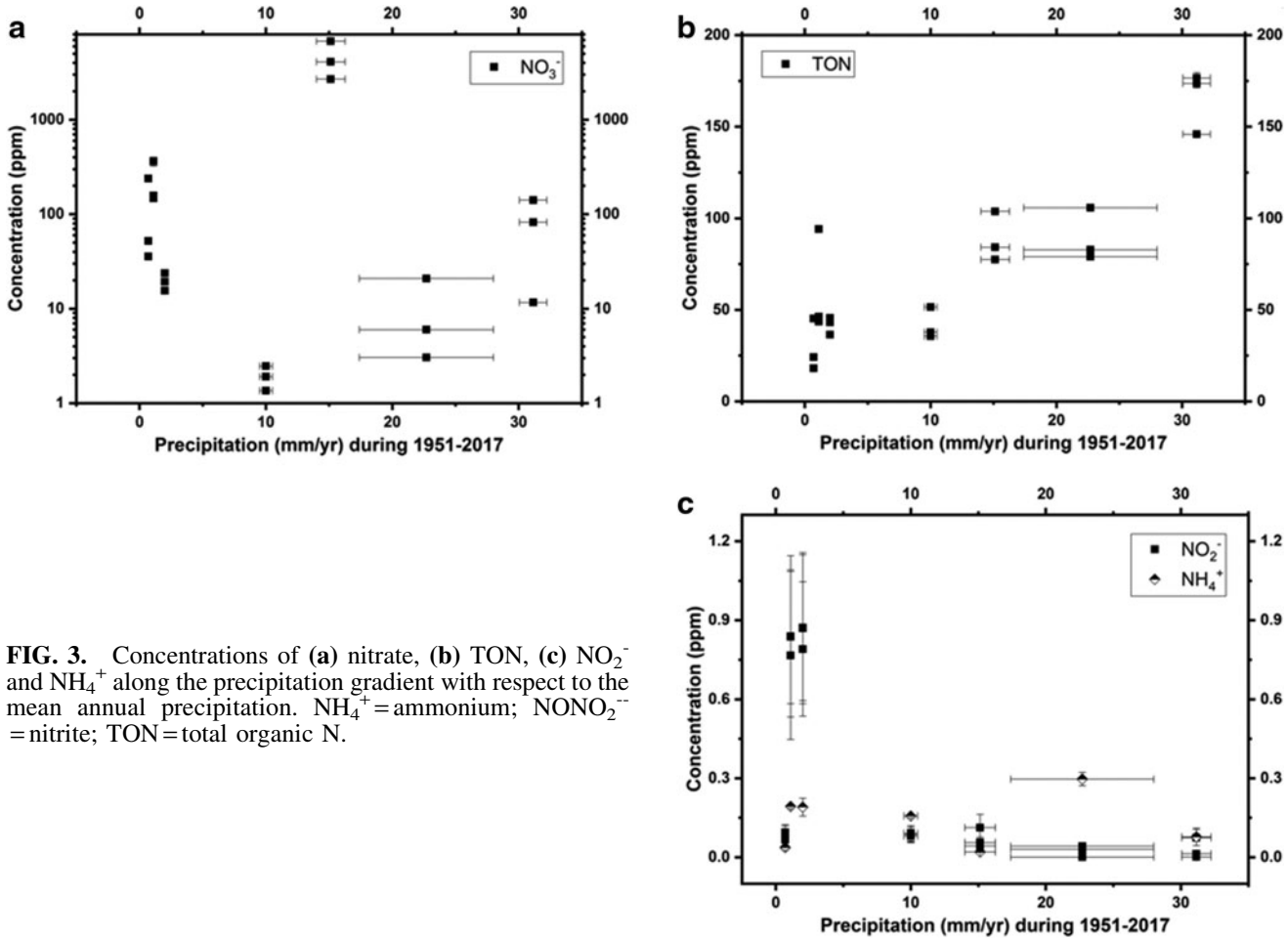

FIG. 3. Concentrations of **(a)** nitrate, **(b)** TON, **(c)** NO_2^- and NH_4^+ along the precipitation gradient with respect to the mean annual precipitation. NH_4^+ = ammonium; $NONO_2^{--}$ = nitrite; TON = total organic N.

higher. Besides, no nitrification pathway was inferred from metagenomic analyses of these Atacama microbial communities (Fig. 6), but alternative nitrate production pathways could additionally supplement the nitrate pool. According to the predicted enzymes (Fig. 7), NO_2^- oxidoreductase that is involved in classical nitrification did not exist, but nitric oxide dioxygenase that oxidizes nitric oxide to nitrate was present (Igamberdiev *et al.*, 2006). Therefore, two alternative nitrification pathways that produce nitric oxide could contribute to the nitrate: (1) nitric oxide synthase could generate nitric oxide by using organic N as substrates (Gusarov *et al.*, 2008); (2) ammonia monooxygenase or hydroxylamine reductase followed by hydroxylamine dehydrogenase could generate nitric oxide from ammonia (Hooper and Terry, 1979) dissociated from organic N by ammonia lyases (Scarlett and Turner, 1976; Kyndt *et al.*, 2002) (Fig. 5f).

Microbial nitrate production follows the mass-dependent fractionation effect on O isotopes, and thus the lower $\delta^{18}O_{NO3}$ and $\Delta^{17}O_{NO3}$ values in transitional and arid sites reflect the biological incorporation of local water sources that are usually $\delta^{18}O$-depleted (Reich and Bao, 2018; Shen *et al.*, 2020). In addition, nitrification regularly overwrites the isotopic signal of increased $\delta^{18}O$ by denitrification (Granger and Wankel, 2016) (Fig. 1). However, in dry soils, denitrification might not always increase nitrate $\delta^{18}O$, since at slow denitrification rates, NO_2^- can react with ambient water to inversely produce nitrate (Casciotti, 2009; Reich and Bao, 2018). After a prolonged period, O isotopes in nitrate will achieve an equilibrium state with O in the ambient water. The average $\delta^{18}O_{NO3}$ and $\Delta^{17}O_{NO3}$ values measured in the transitional and arid sites of this study were $28.0 \pm 5.9‰$ and $7.7 \pm 2.3‰$, respectively, and likely reflect this equilibrium (Table 2).

The $\delta^{15}N$ values of nitrate, on the contrary, should generally increase during biological cycling since the lighter N isotope is preferred in biological reactions (Fig. 1), particularly in the absence of other more exchangeable nitrogenous compounds (Reich and Bao 2018). Accordingly, the increase of $\delta^{15}N_{NO3}$ values in the transitional and arid sites (Table 2 and Fig. 5a) reflects biological nitrate consumption and N loss, including denitrification and nitrate assimilation (Schatz *et al.*, 2011). $\delta^{15}N_{NO3}$ values near 0‰ ($-0.9 \pm 1.2‰$) in hyperarid sites indicated that the microbial activity of nitrate consumption was minimal or much reduced (Bohlke *et al.*, 1997; Michalski *et al.*, 2004; Ewing *et al.*, 2007; Melchiorre *et al.*, 2018). Conversely, the $\delta^{15}N_{NO3}$ values of TZ-5 were 3.3–5.6‰ lower than TZ-4 and TZ-6, which can probably be attributed to lower microbial denitrification activity along with higher alternative nitrification activity, as evidenced by the highest proportions of nitric oxide synthase and dioxygenase in TZ-5 (Fig. 7 and Table 3).

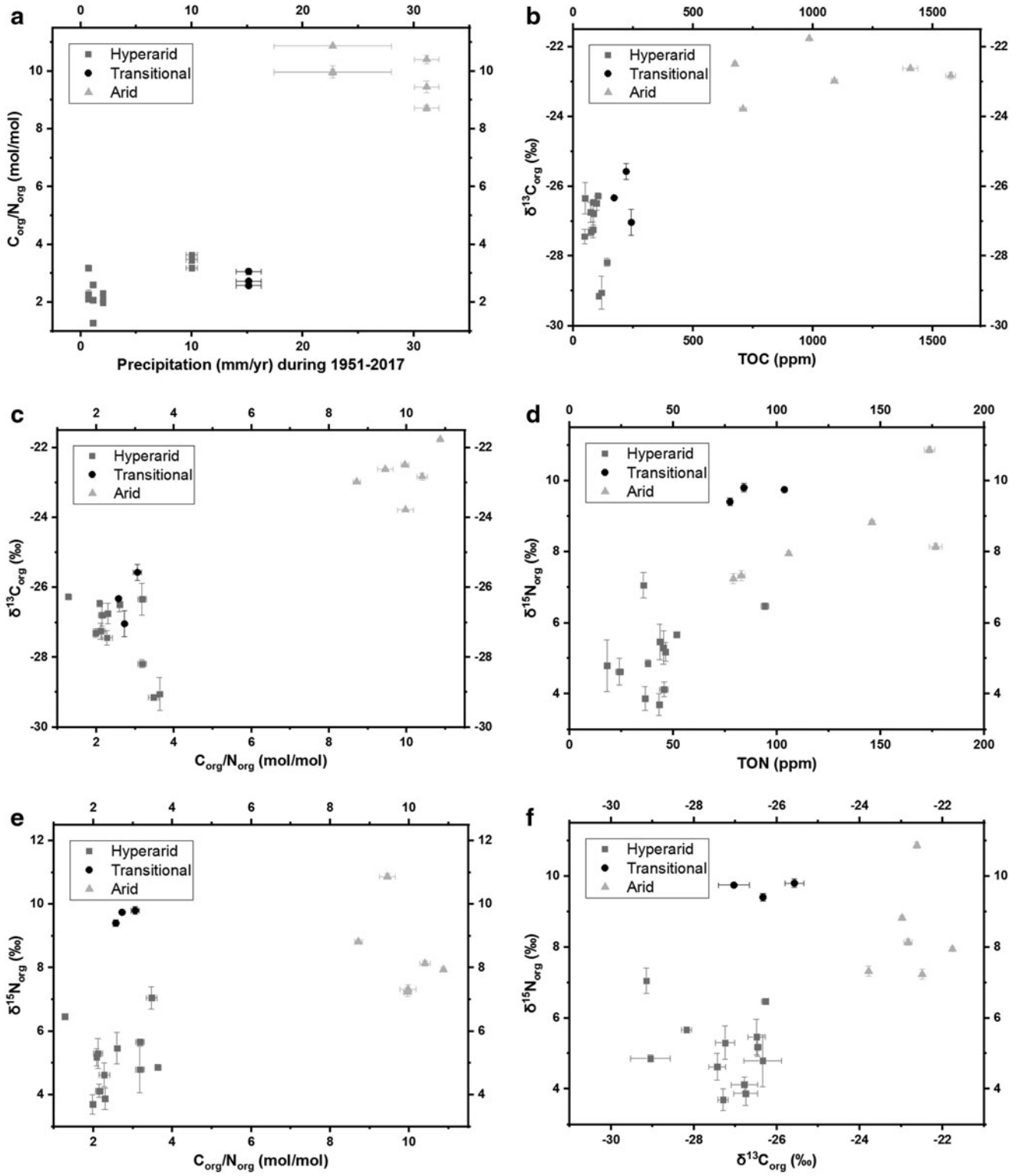

FIG. 4. **(a)** Organic C/N molar ratios of Atacama soils along the latitudinal precipitation gradient. **(b)** Stable organic C isotopes versus TOC. **(c)** Stable organic C isotopes versus C/N ratios. **(d)** Stable N isotopes of organic N versus TON. **(e)** Stable organic N isotopes versus C/N ratios. **(f)** Stable organic N isotopes versus stable organic C isotopes. C/N, carbon-to-nitrogen.

In extracellular environments, ammonium salts are mostly volatilized under the alkaline conditions of the Atacama Desert, and only a small background amount of ammonium is left in the shallow subsurface soils (Fig. 3c) (Ehleringer *et al.*, 1992; Ewing *et al.*, 2007; Orlando *et al.*, 2010; Shen *et al.*, 2019). On the contrary, the external NO_2^- content increased in the two hyperarid sites (PONR and Yungay) that received 20–30 mm precipitation within 2 days about half a year before sampling (Azua-Bustos *et al.*, 2018; Shen *et al.*, 2019). These NO_2^- salts should be primarily

Table 2. Nitrate Stable Isotope Values, the Percentage of Total Soil Nitrate That Is Atmospheric (Assuming 100% Atmospheric Nitrate = 22.9‰ $\Delta^{17}O_{NO3}$), and the Difference Between $\delta^{15}N_{ORG}$ and $\delta^{15}N_{NO3}$ in Atacama Soils Examined in This Study

Site	$\delta^{18}O_{NO3}$ (‰)	$\Delta^{17}O_{NO3}$ (‰)	$\delta^{15}N_{NO3}$ (‰)	NO_2^-/NO_3^- (ppm/ppm)	% atmospheric NO_3^-	$\delta^{15}N_{org}$–$\delta^{15}N_{NO3}$ (‰)
M1	66.9	22.1	0.3	2.7×10^{-3}	96	4.5
M2	60.1	20.9	0.7	2.8×10^{-4}	91	4.6
M3	64.2	21.3	1.1	1.7×10^{-3}	93	3.5
P1	69.4	22.1	–0.1	5.7×10^{-3}	96	5.2
P2	70.6	22.9	0.1	2.1×10^{-3}	100	6.4
P3	64.8	19.8	–0.7	5.3×10^{-3}	86	6.1
Y1	73.6	22.7	–1.5	3.3×10^{-2}	99	5.2
Y2	69.8	21.0	–1.1	4.5×10^{-2}	92	5.0
Y3	68.1	22.7	–2.4	5.6×10^{-2}	99	6.5
T01	63.4	20.2	–1.6	4.8×10^{-2}	88	6.5
T02	70.3	22.6	–2.5	6.0×10^{-2}	98	8.2
T03	66.6	22.4	–2.6	3.5×10^{-2}	98	9.7
T41	26.7	7.0	5.5	1.6×10^{-5}	30	4.3
T42	25.8	7.1	6.0	1.7×10^{-5}	31	3.7
T43	27.2	7.3	5.8	1.4×10^{-5}	32	3.7
T51	30.1	8.4	1.8	1.0×10^{-2}	37	5.5
T52	39.4	9.1	1.6	1.1×10^{-4}	40	5.7
T53	26.6	12.3	2.1	2.0×10^{-3}	54	5.8
T61	17.5	6.1	7.1	6.4×10^{-3}	27	1.7
T62	23.9	3.3	5.4	9.7×10^{-5}	14	2.7
T63	34.5	8.8	6.3	1.6×10^{-5}	38	4.6

generated from the nitrate reductase catalysis, because the NO_2^- generated by hydroxylamine dehydrogenase was usually further processed through nitrifier denitrification intracellularly and both ammonia monooxygenase and hydroxylamine reductase were absent in the more northern hyperarid sites (Table 3).

To summarize (Fig. 8), the atmospheric nitrate deposits without biological disturbance have a low/near-zero $\delta^{15}N_{NO3}$ and high $\delta^{18}O_{NO3}$ (60–75‰). As microbial activity increases in wetter sites, the $\delta^{15}N_{NO3}$ values increase due to intensified denitrification, and the $\delta^{18}O_{NO3}$ values shift toward the slightly negative desert rain $\delta^{18}O_{H2O}$ values (Aravena *et al.*, 1999; Reich and Bao, 2018; Jordan *et al.*, 2019) due to more frequent nitrate/water O exchange triggered by alternative nitrification, assimilation, and denitrification. Melchiorre *et al.* (2018) documented similar trends in nitrate stable isotopes with depth in Atacama soils. These authors showed that, on a 10–200-cm-depth scale, deeper nitrate deposits generally demonstrated abiotic isotope signatures, while shallower deposits demonstrated increasing biological activity. Thus, more abiotic endmembers might be observed deeper into Caliche or Coba layers even in the transitional and arid sites of this study, possibly due to limited moisture penetration beyond a certain depth or texture in Atacama nitrate deposits (Melchiorre *et al.*, 2018). As $\Delta^{17}O_{NO3}$ strongly correlates with $\delta^{18}O_{NO3}$ (Fig. 5c), the plot of $\Delta^{17}O_{NO3}$ versus $\delta^{15}N_{NO3}$ was not elucidated. In addition, the slope of $\Delta^{17}O_{NO3}$-$\delta^{18}O_{NO3}$ linear regressive model was <1, and $\delta^{18}O_{NO3}$ could magnify the difference between abiotic and biogenic signatures for possible martian biomarker detection.

4.2. Corresponding biosignatures in organic matter

$\delta^{13}C$ provides an additional tool in studying microbial carbon and nutrient cycling. $\delta^{13}C$ values in organic carbon largely reflect the dominant type of autotroph and associated carbon dioxide (CO_2) fixation pathway in the ecosystem, namely photosynthetic bacteria, heterotrophic bacteria, algae, three-carbon (C_3) plants, four-carbon (C_4) plants, and Crassulacean acid metabolism (CAM) plants. In the Atacama Desert, most plants that inhabit sandy soils in the south are C_4 grass plants (Quade *et al.*, 2007). The C_4 grass plants have higher $\delta^{13}C_{org}$ values than C_3 and CAM plants and various bacteria, with a mean value of −12‰ (Hamilton and Lewis, 1992; Schidlowski, 2001; Zerkle *et al.*, 2005). Besides these plants, autotrophic microorganisms could also have been an important supply of organic matter to the sediments. Accordingly, our $\delta^{13}C$ results suggest that organic matter in Atacama soils was largely derived from local microbial sources (Ewing *et al.*, 2008; Perez-Fodich *et al.*, 2014) with a $\delta^{13}C_{org}$ of -27.1 ± 1.0‰ (Table 1 and Fig. 4b). In the arid sites, $\delta^{13}C_{org}$ values of -22.7 ± 0.6‰ suggest a mixture of carbon from terrestrial C_4 plants and microbial biomass (Muller, 1977; Prahl *et al.*, 1994; Meyers and Doose, 1999; Melchiorre *et al.*, 2018) (Fig. 4a–c).

Microbial organic carbon can be synthesized or utilized in different N cycling processes. For instance, (1) nitrifying bacteria usually utilize CO_2 as the C source for growth (Marsh *et al.*, 2005). Since atmospheric CO_2 has much higher $\delta^{13}C$ values (−7‰ to −6‰) than local microbial sources (Hare *et al.*, 2018), $\delta^{13}C_{org}$ tends to increase as the nitrification activity increases. (2) Denitrifying bacteria utilize their own organic C as the electron donor (Carlson and Ingraham, 1983). As microorganisms prefer to process lighter organic C isotopes, soil $\delta^{13}C_{org}$ again tends to rise with the increasing microbial abundance and denitrification activity (Knief *et al.*, 2020). Hence, increasing $\delta^{13}C_{org}$ in our samples from the hyperarid to arid sites suggests corresponding increases in the nitrification and denitrification activity (Fig. 4b), which was also supported by the

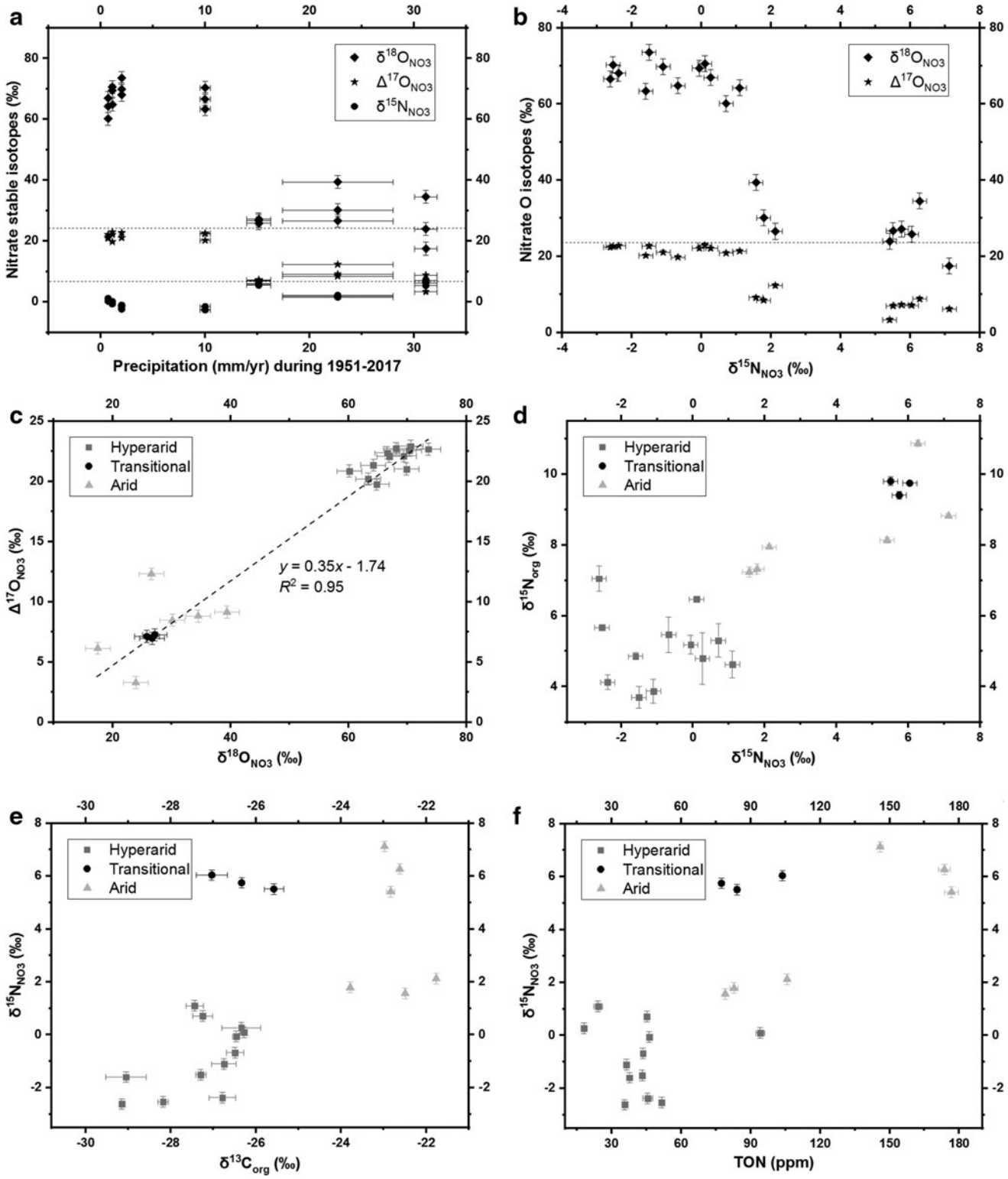

FIG. 5. **(a)** Nitrate stable isotopes in Atacama soils along the latitudinal precipitation gradient. **(b)** Nitrate O isotopes versus nitrate N isotopes. Dotted lines in (**a**) and (**b**) roughly separate the plots of $\delta^{18}O$, $\Delta^{17}O$, and $\delta^{15}N$. **(c)** Nitrate $\Delta^{17}O$ versus nitrate $\delta^{18}O$. **(d)** Stable organic N isotopes versus nitrate N isotopes. **(e)** Nitrate N isotopes versus stable organic C isotopes. **(f)** Nitrate N isotopes versus TON.

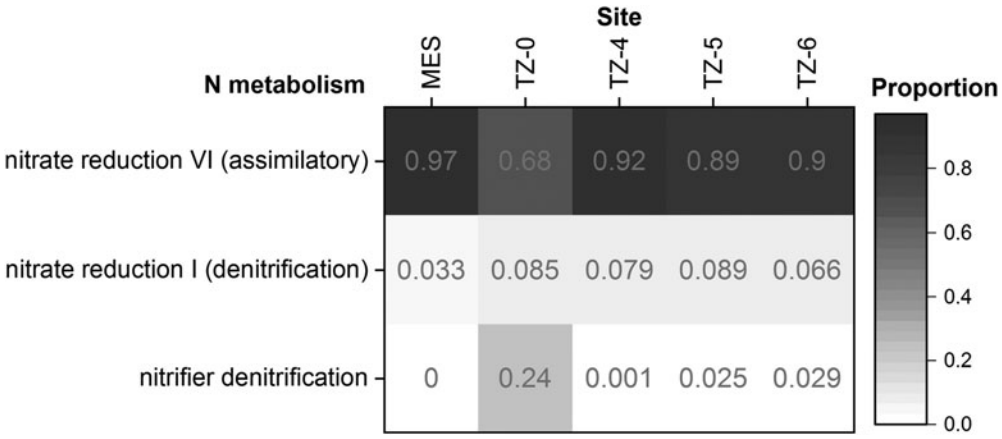

FIG. 6. Proportions of predicted N-processing pathways in microbial N cycling.

significant correlations between $\delta^{15}N_{NO3}$ and $\delta^{13}C_{org}$ ($\rho = 0.71^{**}$, $p = 0.001$, Fig. 5e) as well as TOC ($\rho = 0.61^{**}$, $p = 0.008$).

In contrast to the $\delta^{13}C_{org}$ values that largely reflect the original sources of organic carbon, $\delta^{15}N_{org}$ was more sensitive to recent microbiological activity, as shown by trends in $\delta^{15}N_{org}$ versus C/N ratios and $\delta^{13}C_{org}$ in transitional site TZ-4 (Fig. 4e, f). Given the absence of appreciable ammonium in Atacama soils, organic N would be dominantly generated via nitrate assimilation and nitrogen fixation. However, the proportion of nitrogenase was very low in these soils (Fig. 7 and Table 3), and nitrogen fixation only causes ±2‰ fractionations in $\delta^{15}N$ (Zerkle *et al.*, 2008; Nishizawa *et al.*, 2014; Stueken *et al.*, 2016), as opposed to the >3.5‰ $\delta^{15}N_{org}$ values we measured. Therefore, most of the organic N in Atacama soils was likely formed via nitrate assimilation (Shen *et al.*, 2019).

Despite the high nitrate concentrations in these soils, lack of rainfall leads to low overall N bioavailability, and thus, fractionation effects produced during nitrate uptake and other N transformations are expected to be much lower, due to complete consumption (Supplementary Fig. S1a, b). In addition, since NO_2^- in the hyperarid sites could only be produced as a by-product of assimilatory nitrate reduction, increasing levels of assimilatory nitrate reduction at PONR and Yungay sites that received the most rainfall should result in a corresponding increase in NO_2^- concentrations. As NO_2^- availability became higher in hyperarid sites, the resulting $\delta^{15}N_{org}$ did not decrease by >1‰ (Table 1 and Supplementary

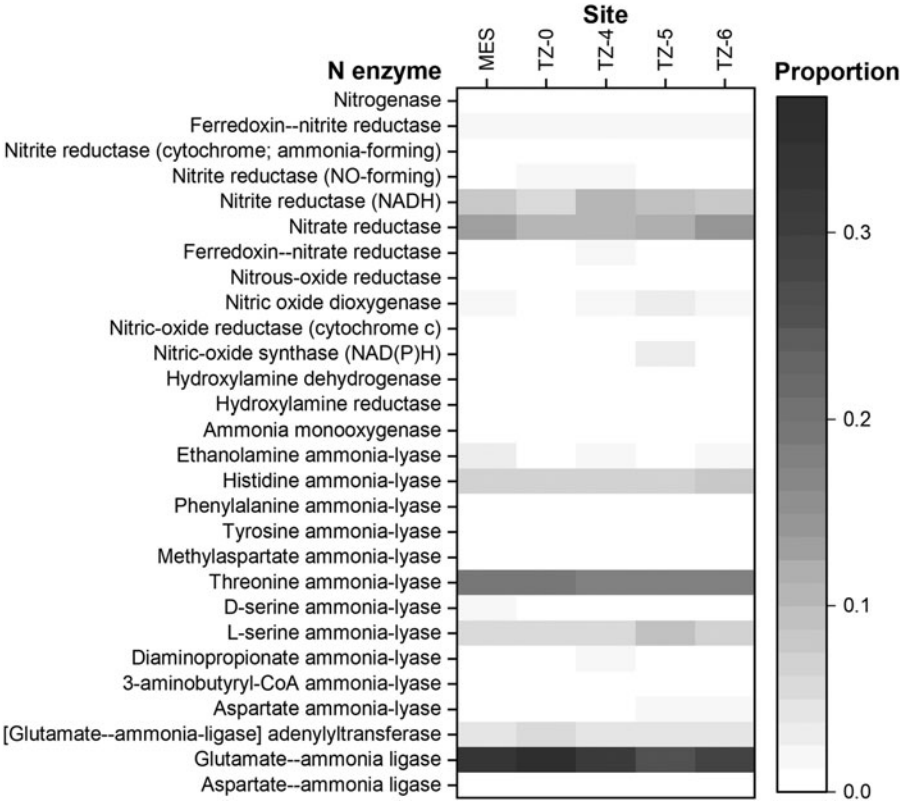

FIG. 7. Proportions of predicted N-processing enzymes in microbial N cycling.

Table 3. Percentages of Each Class of N-Processing Enzyme

Enzymes	*MES*	*TZ-0*	*TZ-4*	*TZ-5*	*TZ-6*
Nitrogenase	0.2%	0.06%	0.04%	0.1%	0.2%
Nitrite reductases	10.6%	9.8%	14.1%	12.0%	11.1%
Nitrate reductases	13.5%	11.1%	11.4%	12.7%	13.9%
Nitrous oxide reductase	0.08%	0.2%	0.2%	0.5%	0.4%
Nitric oxide dioxygenase	1.5%	0.3%	1.5%	3.3%	2.0%
Nitric oxide reductase	0.05%	0.9%	0.1%	0.2%	0.1%
Nitric oxide synthase	0.02%	0.03%	0.03%	2.6%	1.0%
Hydroxylamine dehydrogenase	n.a.	0.8%	0.001%	0.05%	0.05%
Hydroxylamine reductase	0.2%	0.03%	0.02%	0.6%	0.3%
Ammonia monooxygenase	n.a.	0.8%	0.001%	0.05%	0.05%
Ammonia lyases	36.6%	33.0%	36.8%	38.4%	36.7%
Ammonia ligases	37.2%	42.9%	35.7%	29.4%	34.2%

n.a. = not applicable.

Fig. S1d). Thus, the observed $^{15}\varepsilon$ of nitrate assimilation was negligible, although it could decrease when nitrate is solubilized during rainfall.

Intriguingly, despite the small to negligible $^{15}\varepsilon$ we infer for nitrate assimilation, the $\delta^{15}N_{org}$ values were consistently significantly higher than $\delta^{15}N_{NO3}$ (*standardized Wilcoxon signed rank statistic* = 4.02***, $p < 0.001$) (Tables 1, 2, and Fig. 5d), implying that additional pathways and enzymes were involved in organic N transformations. Metagenomic analyses indicate the presence of ammonia lyases and nitric oxide synthase (Table 3), which transform organic N into ammonia and nitric oxide, respectively. Ammonia could then be oxidized to hydroxylamine that could be further oxidized to nitric oxide or NO_2^- by hydroxylamine dehydrogenase. Subsequently, NO_2^- would be denitrified to N_2 through NO_2^- reductase, nitric oxide reductase, and N_2O reductase (Fig. 7 and Table 3). These processes assembled form the complete pathway of nitrifier denitrification (Fig. 6). The intermediate product, nitric oxide, could be reduced to N_2, oxidized to nitrate by nitric oxide dioxygenase, or diffused to the atmosphere. The metagenomic analyses further suggest that nitrifier denitrification and nitric oxide dioxygenase-driven alternative nitrifications increased when TON and $\delta^{15}N_{org}$ increased (Figs. 4d and 7, and Table 3) (Knief *et al.*, 2020).

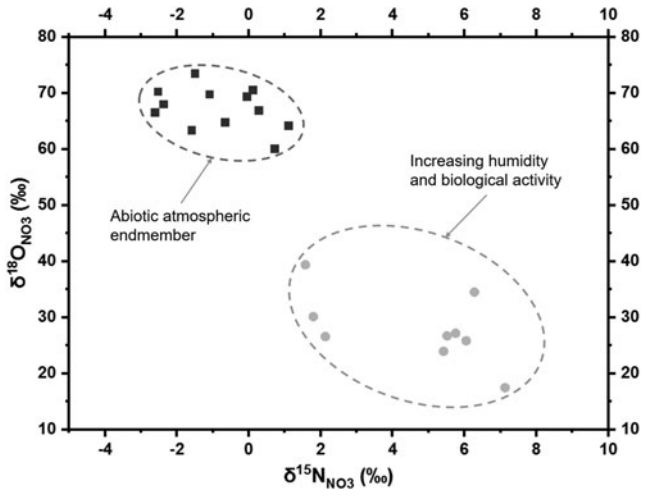

FIG. 8. Differentiation between the abiotic signature of atmospheric endmember and the biogenic signature with increasing annual precipitation based on $\delta^{18}O_{NO3}$ versus $\delta^{15}N_{NO3}$ plot.NO3

Since organic N was mostly produced by nitrate assimilation with minimal $^{15}\varepsilon$, the baseline $\delta^{15}N_{org}$ value should be similar to the residual $\delta^{15}N_{NO3}$ after denitrification. We observed a fairly constant difference of $5.2 \pm 1.7‰$ between $\delta^{15}N_{org}$ and $\delta^{15}N_{NO3}$ values among all sites (Table 1 and Table 2), which indicated a similar expression level of these alternative microbial organic N transformations. For example, the TZ-0 samples had the largest difference between $\delta^{15}N_{org}$ and $\delta^{15}N_{NO3}$ (Table 2), because site TZ-0 had the most dominant nitrifier denitrification compared with other sites (Fig. 6), indicating that organic N was fractionated in $\delta^{15}N$ during conversion to gaseous N_2. TZ-4, on the contrary, had the smallest difference between $\delta^{15}N_{org}$ and $\delta^{15}N_{NO3}$, probably due to the inhibition of nitrifier denitrification or alternative nitrification pathways by its extremely high nitrate concentrations (Fig. 3a).

4.3. N cycling models

Based on these coupled geochemical and metagenomic data, we suggest three separate models for nitrogen cycling in Atacama soils, as summarized in Fig. 9. Denitrification was almost absent in all four hyperarid sites (Fig. 9a, b), but organic N alterations catalyzed by ammonia lyases and nitric oxide synthase resulted in an increase in $\delta^{15}N_{org}$ over background nitrate isotope values. The volatilization of ammonia and nitric oxide is a driver for increasingly heavy $\delta^{15}N_{org}$ values, despite the minimal fractionation effect inferred for ammonia lyase-driven mineralization (Supplementary Fig. S1c). Based on the difference between $\delta^{15}N_{org}$ and $\delta^{15}N_{NO3}$ values in the more northern hyperarid sites (MES, PONR, and Yungay), we estimate $^{15}\varepsilon$ of 3.5‰ to 6.5‰ for these processes (Table 2). In the southern hyperarid site (TZ-0), nitrifier denitrification is an additional organic N loss pathway. Assuming the intensity of ammonia lyase- and nitric oxide synthase-driven organic N loss in TZ-0 was similar to other hyperarid sites, the inferred $^{15}\varepsilon$ of nitrifier denitrification was estimated to range from 2‰ to 6‰ (Fig. 9b).

Within the transitional and arid sites, nitrate assimilation, denitrification, and alternative nitrification reached a steady

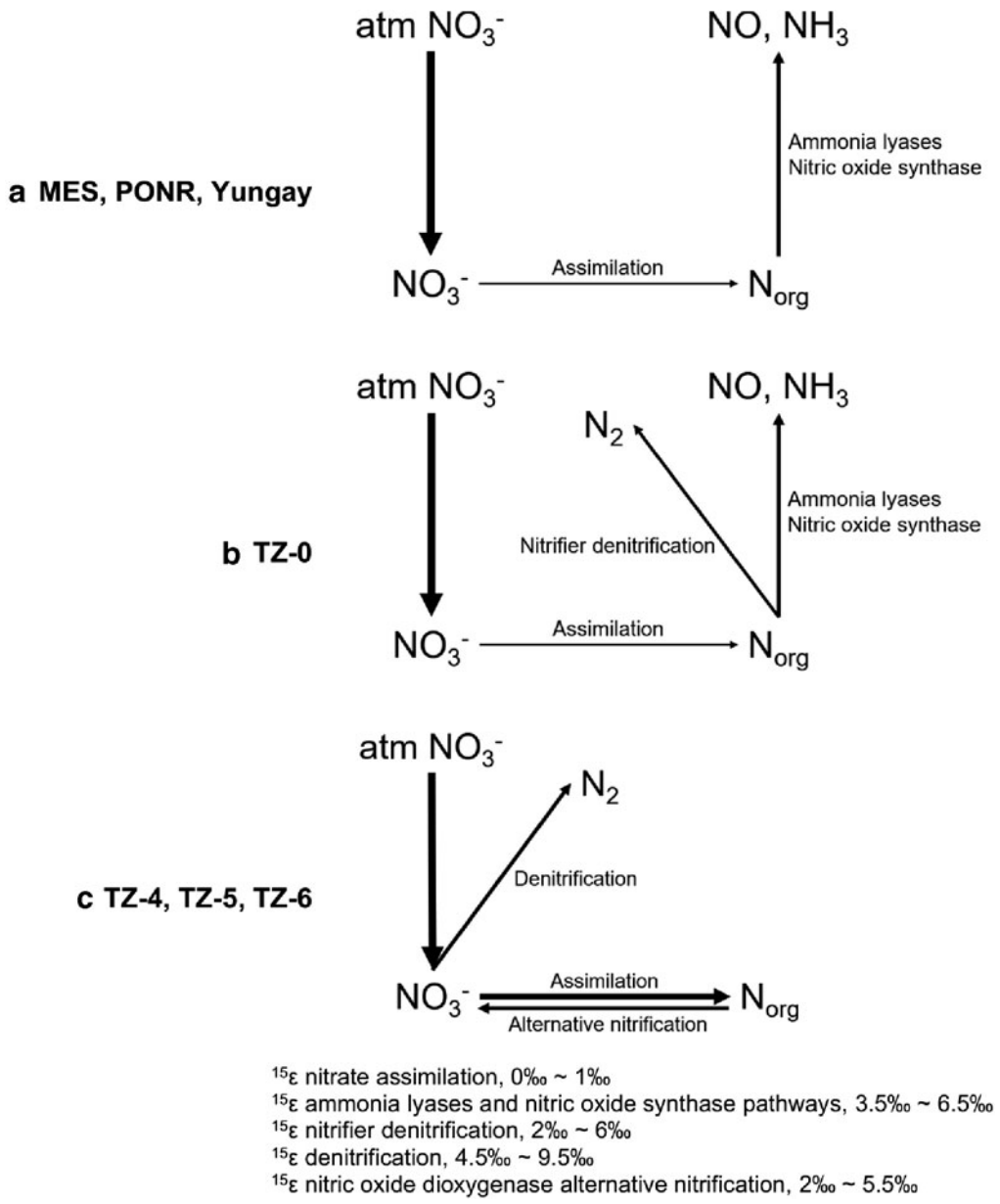

FIG. 9. N cycling models and inferred isotopic enrichment values $^{15}\varepsilon$ in **(a)** the more northern hyperarid regions, **(b)** the southern hyperarid regions, and **(c)** the transitional-arid regions of the Atacama Desert. The thickness of arrows roughly represents the microbial activity of relevant pathways, based on both metagenomic and isotopic data. ''atm NO_3^-''is atmospheric nitrate.

state of biological exchange between O atoms of nitrate and ambient water molecules as supported by the equilibrium $\delta^{18}O_{NO3}$ and $\Delta^{17}O_{NO3}$ values (Fig. 5a, b). O isotope fractionations in nitrate $\delta^{18}O$ of up to 30–40‰ approach equilibrium values set by that of local water sources (Michalski *et al.*, 2012). The increasing $\delta^{15}N_{NO3}$ in these soils primarily reflected the activity of denitrification. Comparing the $\delta^{15}N_{NO3}$ in the transitional-arid sites and in the hyperarid sites, the inferred $^{15}\varepsilon$ of denitrification was from 4.5‰ to 9.5‰.

Nitrifier denitrification by nitrifying bacteria in the transitional and arid sites was shifted to alternative nitrification pathways (Wrage *et al.*, 2001; Zhu *et al.*, 2013) (Fig. 6). The products of ammonia lyases and nitric oxide synthase would also be more actively involved in the intracellular alternative nitrification pathways (Fig. 9c). Therefore, the increase in $\delta^{15}N_{org}$ in these sites can be attributed primarily to alternative nitrification pathways with an inferred $^{15}\varepsilon$ of 2‰ to 5.5‰ (Michalski *et al.*, 2012). Furthermore, nitrogen cycling was heterogeneous in each sampling site. For example, assimilatory nitrate reduction was stronger in PONR and Yungay, with higher NO_2^- concentrations than in the other hyperarid sites; TZ-4 had slightly lower expression of alternative nitrification pathways than TZ-5 and TZ-6, possibly due to product inhibition; and TZ-5 might have a lower microbial denitrification activity and/or a higher alternative nitrification activity, in comparison.

To move the findings of this study forward, we may apply our determined nitrate biosignatures in the future martian

soil analysis interpretation. On early Mars (Noachian and early Hesperian Periods), life may have thrived if liquid water was abundant as evidenced by the trace of outflow channels, ocean basins, deltaic deposits, and fan-shaped aprons (Irwin *et al.*, 2002; Malin and Edgett, 2003; Carr and Head, 2010; Di Achille and Hynek, 2010; Hynek *et al.*, 2010). Microbial life that could cycle nitrate might exist and perform denitrification- and nitrification-like processes, leaving traceable elevated $\delta^{15}N_{NO3}$ and altered $\delta^{18}O_{NO3}$ markers that had been buried in deep subsurface since the Hesperian Period.

As for the more recent hyperarid Mars, the formation of a subsurface thin layer of liquid water can be promoted by diurnal cycles (Anderson and Tice, 1979; Martin-Torres *et al.*, 2015) and can be retained by hydrated minerals (Davila *et al.*, 2010; Meslin *et al.*, 2013). In addition, a recent radar survey has detected an appreciable subglacial liquid water repository on the current Mars (Orosei *et al.*, 2018). Thus, if these water sources could support emergent martian microorganisms that cycled essential elements, they would likely consume the abundant nitrate as nutrient (Shen *et al.*, 2019) and could potentially produce detectable geochemical biomarkers. Although this study suggests that the hyperarid core of the Atacama Desert preserves the abiotic atmospheric nitrate signature, putative microorganisms on Mars could perform nitrate/water O exchange by nitrate assimilation when ambient moisture rises to a suitable level for this metabolism. This O exchange activity could then shift nitrate O isotope ratios toward those of water.

It is noteworthy that enzymes and pathways discussed in this article are identified via the database-based metagenome function inference method. No matter how robust and valid the PICRUSt2 inference algorithm is, further transcriptomic, proteomic, or metabolomic analyses (Haider and Pal, 2013; Seyler *et al.*, 2020) could be conducted in the future and optimize the arguments made in this study.

5. Conclusions

Nitrate and organic matter in Atacama soils are broadly affected by an assortment of microbial N dynamics, abiotic processes, and the intensity of different enzyme expressions, all of which are manifested in their C, N, and O stable isotope records. Although we have documented some microbial activity, nitrates in the hyperarid sites with an annual precipitation of <10 mm have $\delta^{15}N$, $\delta^{18}O$, and $\Delta^{17}O$ values that largely reflect their atmospheric source, with little biological influence.

Stable isotope signatures of nitrates from the transitional and arid sites with >15 mm annual precipitation are overprinted by biologically driven enrichment in $\delta^{15}N_{NO3}$ and nitrate/water equilibrium in $\delta^{18}O_{NO3}$ and $\Delta^{17}O_{NO3}$. Increasing $\delta^{15}N_{NO3}$ in transitional and arid sites primarily reflects enhanced denitrification. Nitrate assimilation with seemingly minimal stable isotope effects is the only nitrate consumption pathway in the hyperarid sites, while ammonia lyase- and nitric oxide synthase-driven organic N loss leads to an increase in hyperarid $\delta^{15}N_{org}$. Nitrifier denitrification further increases the $\delta^{15}N_{org}$ values in the southernmost hyperarid site, but nitric oxide dioxygenase-driven alternative nitrification pathways dominate the transitional and arid sites. Notably, stable isotope fractionations expressed by these N transformations are all at the low end of what has previously been proposed for these processes, due to the low bioavailability of N sources.

We have demonstrated that the effects of water and microbial activity impart measurable differences in proxies (*e.g.*, $\delta^{18}O_{NO3}$ or $\Delta^{17}O_{NO3}$ vs. $\delta^{15}N_{NO3}$, $\delta^{13}C_{org}$ or $\delta^{15}N_{org}$ vs. C_{org}:N_{org}), across a gradient of habitability in desert soils. Soils in the driest regions reflect predominantly an abiotic atmospheric endmember, but in themselves do not constitute an antibiosignature. However, we interpret the spread in isotopic values away from the atmospheric endmember as a clear biosignature for enhanced microbial processing in wetter (although still extremely arid) soils, demonstrating that relatively simple geochemical measurements (which could be performed robotically) distinguish biogenic processing in dry soils as they move through various regimens toward full biogeochemical nitrogen cycling. We speculate that extinct or potentially extant martian microorganisms may consume atmospheric nitrate via assimilation, and that isotopic variation in nitrates and organic matter could be biosignatures in martian soils indicating where the moisture content is (or was) intermittently relatively high.

Data Availability

The raw sequencing data for enzyme and functional pathway inferences in this study are stored in the National Center for Biotechnology Information (NCBI) under the BioProject ID PRJNA595740.

Acknowledgments

We thank Adam Wyness from Scottish Oceans Institute, School of Biology, University of St Andrews, St Andrews KY16 8LB, UK, and the Department of Zoology and Entomology, Rhodes University, Grahamstown 6139, South Africa, for assisting the soil DNA extractions. We also thank Jan Kaiser and Sarah Wexler from Science Analytical Facility, University of East Anglia, Norwich NR4 7TJ, UK, for nitrate stable isotope measurements.

Author Disclosure Statement

No competing financial interests exist.

Funding Information

This research was funded by the European Research Council (ERC) under the European Union's Horizon 2020 Research and Innovation Programme (grant agreement 678812) (to M.W.C.). J.S. also acknowledges support from the China Scholarship Council (CSC).

Supplementary Material

Supplementary Figure S1

References

Anderson DM and Tice AR (1979) Analysis of water in the Martian regolith. *J Mol Evol* 14:33–38.

Aravena R, Suzuki O, Pena H, *et al.* (1999) Isotopic composition and origin of the precipitation in Northern Chile. *Appl Geochem* 14:411–422.

Azua-Bustos A, Fairen AG, Gonzalez-Silva C, *et al*. (2018) Unprecedented rains decimate surface microbial communities in the hyperarid core of the Atacama Desert. *Sci Rep* 8:16706.

Bohlke JK, Ericksen GE and Revesz K (1997) Stable isotope evidence for an atmospheric origin of desert nitrate deposits in northern Chile and southern California, USA. *Chem Geol* 136:135–152.

Boschetti T, Cifuentes J, Iacumin P, *et al*. (2019) Local meteoric water line of Northern Chile (18 degrees S-30 degrees S): an application of error-in-variables regression to the oxygen and hydrogen stable isotope ratio of precipitation. *Water* 11: 791.

Bottcher J, Strebel O, Voerkelius S, *et al*. (1990) Using isotope fractionation of nitrate nitrogen and nitrate oxygen for evaluation of microbial denitrification in a sandy aquifer. *J Hydrol* 114:413–424.

Buchwald C and Casciotti KL (2010) Oxygen isotopic fractionation and exchange during bacterial nitrite oxidation. *Limnol Oceanogr* 55:1064–1074.

Carlson CA and Ingraham JL (1983) Comparison of denitrification by *Pseudomonas stutzeri*, *Pseudomonas aeruginosa*, and *Paracoccus denitrificans*. *Appl Environ Microbiol* 45: 1247–1253.

Carr MH and Head JW (2010) Geologic history of Mars. *Earth Planet Sci Lett* 294:185–203.

Casciotti KL (2009) Inverse kinetic isotope fractionation during bacterial nitrite oxidation. *Geochim Cosmochim Acta* 73: 2061–2076.

Casciotti KL, Sigman DM, Hastings MG, *et al*. (2002) Measurement of the oxygen isotopic composition of nitrate in seawater and freshwater using the denitrifier method. *Anal Chem* 74:4905–4912.

Casciotti KL, McIlvin M and Buchwald C (2010) Oxygen isotopic exchange and fractionation during bacterial ammonia oxidation. *Limnol Oceanogr* 55:753–762.

Casciotti KL, Buchwald C and McIlvin M (2013) Implications of nitrate and nitrite isotopic measurements for the mechanisms of nitrogen cycling in the Peru oxygen deficient zone. *Deep Sea Res Part I Oceanogr Res Papers* 80:78–93.

Catling DC, Claire MW, Zahnle KJ, *et al*. (2010) Atmospheric origins of perchlorate on Mars and in the Atacama. *J Geophys Res Planets* 115:E00E11.

Comer-Warner SA, Gooddy DC, Ullah S, *et al*. (2020) Seasonal variability of sediment controls of nitrogen cycling in an agricultural stream. *Biogeochemistry* 148:31–48.

Davila AF, Duport LG, Melchiorri R, *et al*. (2010) Hygroscopic salts and the potential for life on Mars. *Astrobiology* 10:617–628.

Denk TRA, Mohn J, Decock C, *et al*. (2017) The nitrogen cycle: a review of isotope effects and isotope modeling approaches. *Soil Biol Biochem* 105:121–137.

Di Achille G and Hynek BM (2010) Ancient ocean on Mars supported by global distribution of deltas and valleys. *Nat Geosci* 3:459–463.

Douglas GM, Maffei VJ, Zaneveld J, *et al*. (2019) PICRUSt2: an improved and extensible approach for metagenome inference. *BioRxiv*, DOI: 10.1101/672295.

Ehleringer JR, Mooney HA, Rundel PW, *et al*. (1992) Lack of nitrogen cycling in the atacama desert. *Nature* 359:316–318.

Ericksen GE (1983) The Chilean nitrate deposits. *Am Sci* 71: 366–374.

Ewing SA, Michalski G, Thiemens M, *et al*. (2007) Rainfall limit of the N cycle on Earth. *Glob Biogeochem Cycles* 21: GB3009.

Ewing SA, Yang W, DePaolo DJ, *et al*. (2008) Non-biological fractionation of stable Ca isotopes in soils of the Atacama Desert, Chile. *Geochim Cosmochim Acta* 72:1096–1110.

Fernandez-Remolar DC, Chong-Diaz G, Ruiz-Bermejo M, *et al*. (2013) Molecular preservation in halite- and perchlorate-rich hypersaline subsurface deposits in the Salar Grande basin (Atacama Desert, Chile): implications for the search for molecular biomarkers on Mars. *J Geophys Res Biogeosci* 118:922–939.

Fritz P, Suzuki O, Silva C, *et al*. (1981) Isotope hydrology of groundwaters in the Pampa Del Tamarugal, Chile. *J Hydrol* 53:161–184.

Granger J and Wankel SD (2016) Isotopic overprinting of nitrification on denitrification as a ubiquitous and unifying feature of environmental nitrogen cycling. *Proc Natl Acad Sci U S A* 113:E6391–E6400.

Granger J, Sigman DM, Needoba JA, *et al*. (2004) Coupled nitrogen and oxygen isotope fractionation of nitrate during assimilation by cultures of marine phytoplankton. *Limnol Oceanogr* 49:1763–1773.

Granger J, Sigman DM, Lehmann MF, *et al*. (2008) Nitrogen and oxygen isotope fractionation during dissimilatory nitrate reduction by denitrifying bacteria. *Limnol Oceanogr* 53: 2533–2545.

Granger J, Sigman DM, Rohde MM, *et al*. (2010) N and O isotope effects during nitrate assimilation by unicellular prokaryotic and eukaryotic plankton cultures. *Geochim Cosmochim Acta* 74:1030–1040.

Gusarov I, Starodubtseva M, Wang ZQ, *et al*. (2008) Bacterial nitric-oxide synthases operate without a dedicated redox partner. *J Biol Chem* 283:13140–13147.

Haider S and Pal R (2013) Integrated analysis of transcriptomic and proteomic data. *Curr Genomics* 14:91–110.

Hamilton SK and Lewis Jr. WM (1992) Stable carbon and nitrogen isotopes in algae and detritus from the Orinoco River floodplain, Venezuela. *Geochim Cosmochim Acta* 56:4237–4246.

Hare VJ, Loftus E, Jeffrey A, *et al*. (2018) Atmospheric CO2 effect on stable carbon isotope composition of terrestrial fossil archives. *Nat Commun* 9:252.

Hooper AB and Terry KR (1979) Hydroxylamine oxidoreductase of Nitrosomonas. Production of nitric oxide from hydroxylamine. *Biochim Biophys Acta* 571:12–20.

Hynek BM, Beach M, and Hoke MRT (2010) Updated global map of Martian valley networks and implications for climate and hydrologic processes. *J Geophys Res* 115:E09008.

IBM Corp (2019) *IBM SPSS Statistics for Windows*. IBM Corp., Armonk, NY.

Igamberdiev AU, Baron KN, and Hill RD (2006) Nitric oxide as an alternative electron carrier during oxygen deprivation. In: *Nitric Oxide in Plant Growth, Development and Stress Physiology*, edited by L Lamattina and JC Polacco, Springer, Berlin, Heidelberg, pp 255–268.

Illumina® (2013) 16S Metagenomic Sequencing Library Preparation. Available online at https://support.illumina.com/documents/documentation/chemistry_documentation/16s/16s-metagenomic-library-prep-guide-15044223-b.pdf

Irwin RP, Maxwell TA, Howard AD, *et al*. (2002) A large paleolake basin at the head of Ma'adim Vallis, Mars. *Science* 296:2209–2212.

Jackson WA, Bohlke JK, Andraski BJ, *et al*. (2015) Global patterns and environmental controls of perchlorate and nitrate co-occurrence in arid and semi-arid environments. *Geochim Cosmochim Acta* 164:502–522.

Jaramillo EA, Royle SH, Claire MW, *et al*. (2019) Indigenous organic-oxidized fluid interactions in the Tissint Mars meteorite. *Geophys Res Lett* 46:3090–3098.

Jordan TE, Herrera C, Godfrey LV, *et al*. (2019) Isotopic characteristics and paleoclimate implications of the extreme precipitation event of March 2015 in northern Chile. *Andean Geol* 46:1–31.

Kaiser J, Hastings MG, Houlton BZ, *et al*. (2007) Triple oxygen isotope analysis of nitrate using the denitrifier method and thermal decomposition of N2O. *Anal Chem* 79:599–607.

Knief C, Bol R, Amelung W, Kusch S, *et al*. (2020) Tracing elevational changes in microbial life and organic carbon sources in soils of the Atacama Desert. *Glob Planet Change* 184:103078.

Kohl DH and Shearer G (1980) Isotopic fractionation associated with symbiotic N-2 fixation and uptake of No3—by plants. *Plant Physiol* 66:51–56.

Kounaves SP, Carrier BL, O'Neil GD, *et al*. (2014) Evidence of Martian perchlorate, chlorate, and nitrate in Mars meteorite EETA79001: implications for oxidants and organics. *Icarus* 229:206–213.

Kyndt JA, Meyer TE, Cusanovich MA, *et al*. (2002) Characterization of a bacterial tyrosine ammonia lyase, a biosynthetic enzyme for the photoactive yellow protein. *FEBS Lett* 512:240–244.

Lam P and Kuypers MMM (2011) Microbial nitrogen cycling processes in oxygen minimum zones. *Ann Rev Mar Sci* 3: 317–345.

Malin MC and Edgett KS (2003) Evidence for persistent flow and aqueous sedimentation on early Mars. *Science* 302:1931–1934.

Mariotti A, Mariotti F, Amarger N, *et al*. (1980) Nitrogen isotope fractionation during nitrate absorption and atmospheric nitrogen-fixation by plants. *Physiol Veg* 18:163–181.

Mariotti A, Mariotti F, Champigny ML, *et al*. (1982) Nitrogen isotope fractionation associated with nitrate reductase-activity and uptake of No3- by pearl-millet. *Plant Physiol* 69: 880–884.

Marsh KL, Sims GK and Mulvaney RL (2005) Availability of urea to autotrophic ammonia-oxidizing bacteria as related to the fate of 14 C-and 15 N-labeled urea added to soil. *Biol Fertil Soils* 42:137.

Martin-Torres FJ, Zorzano MP, Valentin-Serrano P, *et al*. (2015) Transient liquid water and water activity at Gale crater on Mars. *Nat Geosci* 8:357–361.

McCready RGL, Gould WD, and Barendregt RW (1983) Nitrogen isotope fractionation during the reduction of NO_3^- to NH_4^+ by *Desulfovibrio* sp. *Can J Microbiol* 29:231–234.

Melchiorre EB and Talyn BC (2014) Nitrogen stable isotope composition and the origins of cupric nitrate mineralization. *Chem Geol* 388:1–8.

Melchiorre EB, Sickman JO, Talyn BC, *et al*. (2018) Isotope stratigraphy: insights on paleoclimate and formation of nitrate deposits in the Atacama Desert, Chile. *J Arid Environ* 148: 45–53.

Meslin PY, Gasnault O, Forni O, *et al*. (2013) Soil diversity and hydration as observed by ChemCam at Gale Crater, Mars. *Science* 341:1238670.

Meyers PA and Doose H (1999) 29. Sources, preservation, and thermal maturity of organic matter in Pliocene-Pleistocene organic-carbon-rich sediments of the western Mediterranean Sea. In *Proceedings of the Ocean Drilling Program: Scientific results. The Program*, Vol. 161, edited by R Zahn, MC Comas, and A Klaus, pp 383–390.

Michalski G, Scott Z, Kabiling M, *et al*. (2003) First measurements and modeling of Delta O-17 in atmospheric nitrate. *Geophys Res Lett* 30, DOI: 10.1029/2003GL017015.

Michalski G, Bohlke JK, and Thiemens M (2004) Long term atmospheric deposition as the source of nitrate and other salts in the Atacama Desert, Chile: new evidence from mass-independent oxygen isotopic compositions. *Geochim Cosmochim Acta* 68:4023–4038.

Michalski G, Bockheim JG, Kendall C, *et al*. (2005) Isotopic composition of Antarctic Dry Valley nitrate: implications for NOy sources and cycling in Antarctica. *Geophys Res Lett* 32, DOI: 10.1029/2004GL022121.

Michalski G, Bhattacharya SK, and Mase DF (2012) Oxygen isotope dynamics of atmospheric nitrate and its precursor molecules. In *Handbook of Environmental Isotope Geochemistry*, edited by M Baskaran, Springer, Berlin, Heidelberg, pp 613–635.

Michalski G, Bhattacharya SK, and Girsch G. (2014) NOx cycle and the tropospheric ozone isotope anomaly: an experimental investigation. *Atmos Chem Phys* 14:4935–4953.

Montoya J (2008) Nitrogen stable isotopes in marine environments. In *Nitrogen in the Marine Environment* 2nd ed., edited by DG Capone, DA Bronk, MR Mulholland, and EJ Carpenter, Academic Press, London, pp 1277–1302.

Muller PJ (1977) C-N ratios in pacific deep-sea sediments—effect of inorganic ammonium and organic nitrogen-compounds sorbed by clays. *Geochim Cosmochim Acta* 41:765–776.

Nishizawa M, Miyazaki J, Makabe A, *et al*. (2014) Physiological and isotopic characteristics of nitrogen fixation by hyperthermophilic methanogens: key insights into nitrogen anabolism of the microbial communities in Archean hydrothermal systems. *Geochim Cosmochim Acta* 138:117–135.

OriginLab Corp (2019) *Origin(Pro)*. OriginLab Corporation, Northampton, MA.

Orlando J, Alfaro M, Bravo L, *et al*. (2010) Bacterial diversity and occurrence of ammonia-oxidizing bacteria in the Atacama Desert soil during a ''desert bloom'' event. *Soil Biol Biochem* 42:1183–1188.

Orosei R, Lauro SE, Pettinelli E, *et al*. (2018) Radar evidence of subglacial liquid water on Mars. *Science* 361:490–493.

Perez-Fodich A, Reich M, Alvarez F, *et al*. (2014) Climate change and tectonic uplift triggered the formation of the Atacama Desert's giant nitrate deposits. *Geology* 42:251–254.

Prahl FG, Ertel JR, Goni MA, *et al*. (1994) Terrestrial organic-carbon contributions to sediments on the Washington margin. *Geochim Cosmochim Acta* 58:3035–3048.

Qin Y, Li YH, Bao HM, *et al*. (2012) Massive atmospheric nitrate accumulation in a continental interior desert, northwestern China. *Geology* 40:623–626.

Quade J, Rech JA, Latorre C, *et al*. (2007) Soils at the hyperarid margin: the isotopic composition of soil carbonate from the Atacama Desert, Northern Chile. *Geochim Cosmochim Acta* 71:3772–3795.

Rech JA, Currie BS, Michalski G, *et al*. (2006) Neogene climate change and uplift in the Atacama Desert, Chile. *Geology* 34: 761–764.

Reich M and Bao HM (2018) Nitrate deposits of the Atacama desert: a marker of long-term hyperaridity. *Elements* 14:251–256.

Scarlett FA and Turner JM (1976) Microbial metabolism of amino alcohols. Ethanolamine catabolism mediated by coenzyme B12-dependent ethanolamine ammonia-lyase in *Escherichia coli* and *Klebsiella aerogenes*. *J Gen Microbiol* 95:173–176.

Schatz AK, Zech M, Buggle B, *et al*. (2011) The late quaternary loess record of Tokaj, Hungary: reconstructing

palaeoenvironment, vegetation and climate using stable C and N isotopes and biomarkers. *Quat Int* 240:52–61.
Schidlowski M (2001) Carbon isotopes as biogeochemical recorders of life over 3.8 Ga of Earth history: evolution of a concept. *Precambrian Res* 106:117–134.
Schotterer U, Oldfield F and Fröhlich K (1996) *GNIP. Global Network for Isotopes in Precipitation*. International Atomic Energy Agency, Vienna, Austria.
Sernageomin (2003) Mapa Geológico de Chile: versión digital. *Servicio Nacional de Geología y Minería, Publicación Geológica Digital, No. 4 CD-Room, versión 1.0, base geológica escala* 1. Available online at http://www.ipgp.fr/~dechabal/Geol-millon.pdf
Seyler L, Kujawinski EB, Azua-Bustos A, *et al.* (2020) Metabolomics as an emerging tool in the search for astrobiologically relevant biomarkers. *Astrobiology* 20:1251–1261.
Shen J, Zerkle AL, Stueken EE, *et al*. (2019) Nitrates as a potential n supply for microbial ecosystems in a hyperarid Mars analog system. *Life* 9:79.
Shen J, Smith AC, Claire MW, *et al*. (2020) Unraveling biogeochemical phosphorus dynamics in hyperarid Mars-analogue soils using stable oxygen isotopes in phosphate. *Geobiology* 18: 760–779.
Shen J, Wyness AJ, Claire MW, *et al*. (2021) Spatial variability of microbial communities and salt distributions across a latitudinal aridity gradient in the Atacama Desert. *Microb Ecol* 82:1–17.
Sigman DM, Casciotti KL, Andreani M, *et al*. (2001) A bacterial method for the nitrogen isotopic analysis of nitrate in seawater and freshwater. *Anal Chem* 73:4145–4153.
Sigman DM, Granger J, DiFiore PJ, *et al*. (2005) Coupled nitrogen and oxygen isotope measurements of nitrate along the eastern North Pacific margin. *Glob Biogeochem Cycles* 19, DOI: 10.1029/2005GB002458.
Sigman D, Karsh K, and Casciotti K (2009) Ocean process tracers: nitrogen isotopes in the ocean. In *Encyclopedia of Ocean Sciences*, edited by J Steele, S Thorpe, and K Turekians, Academic Press, Oxford, pp 40–54.
Smith ML, Claire MW, Catling DC, *et al*. (2014) The formation of sulfate, nitrate and perchlorate salts in the Martian atmosphere. *Icarus* 231:51–64.
Stern JC, Sutter B, Freissinet C, *et al*. (2015) Evidence for indigenous nitrogen in sedimentary and aeolian deposits from the Curiosity rover investigations at Gale crater, Mars. *Proc Natl Acad Sci U S A* 112:4245–4250.
Stueken EE, Kipp MA, Koehler MC, *et al*. (2016) The evolution of Earth's biogeochemical nitrogen cycle. *Earth-Sci Rev* 160: 220–239.
Stueken EE, Zaloumis J, Meixnerova J, *et al*. (2017) Differential metamorphic effects on nitrogen isotopes in kerogen extracts and bulk rocks. *Geochim Cosmochim Acta* 217:80–94.
Sun T, Bao HM, Reich M, *et al*. (2018) More than ten million years of hyper-aridity recorded in the Atacama Gravels. *Geochim Cosmochim Acta* 227:123–132.
Tischner R (2000) Nitrate uptake and reduction in higher and lower plants. *Plant Cell Environ* 23:1005–1024.
Vicars WC and Savarino J (2014) Quantitative constraints on the O-17-excess (Delta O-17) signature of surface ozone: ambient measurements from 50 degrees N to 50 degrees S using the nitrite-coated filter technique. *Geochim Cosmochim Acta* 135:270–287.
Wada E and Hattori A (1978) Nitrogen isotope effects in the assimilation of inorganic nitrogenous compounds by marine diatoms. *Geomicrobiol J* 1:85–101.
Walvoord MA, Phillips FM, Stonestrom DA, *et al*. (2003) A reservoir of nitrate beneath desert soils. *Science* 302:1021–1024.
Wrage N, Velthof GL, Van Beusichem ML, *et al*. (2001) Role of nitrifier denitrification in the production of nitrous oxide. *Soil Biol Biochem* 33:1723–1732.
Xu XM, Li Y, Li YZ, *et al*. (2019) Characteristics of desert varnish from nanometer to micrometer scale: a photo-oxidation model on its formation. *Chem Geol* 522:55–70.
Zerkle AL, House CH, and Brantley SL (2005) Biogeochemical signatures through time as inferred from whole microbial genomes. *Am J Sci* 305:467–502.
Zerkle AL, Junium CK, Canfield DE, *et al*. (2008) Production of 15N-depleted biomass during cyanobacterial N2-fixation at high Fe concentrations. *J Geophys Res* 113:G03014.
Zhu X, Burger M, Doane TA, *et al*. (2013) Ammonia oxidation pathways and nitrifier denitrification are significant sources of N2O and NO under low oxygen availability. *Proc Natl Acad Sci U S A* 110:6328–6333.

Address correspondence to:
Jianxun Shen
Centre for Exoplanet Science
School of Earth and Environmental Sciences
University of St Andrews
Irvine Building, North Street
St Andrews KY16 9AL
United Kingdom
USA

E-mail: js365@st-andrews.ac.uk

Submitted 22 January 2021
Accepted 11 September 2021
Associate Editor: Victor Parro

Abbreviations Used

C_3 = three-carbon
C_4 = four-carbon
CAM = Crassulacean acid metabolism
CO_2 = carbon dioxide
CSC = China Scholarship Council
$d^{13}C$ = carbon isotopes
DNRA = dissimilatory nitrate reduction to ammonium
EC = Enzyme Commission
ERC = European Research Council
GC-IRMS = gas chromatography-isotope ratio mass spectrometry
IC = ion chromatography
MES = María Elena South
N = nitrogen
N_2 = dinitrogen gas
N_2O = nitrous oxide
n.a. = not applicable
NCBI = National Center for Biotechnology Information
NH_4^+ = ammonium
NO_2^- = nitrite
O = oxygen
O_3 = ozone
PONR = Point of No Return
TN = total N
TOC = total organic C
TON = total organic N
TZ = Transition Zone
UV = ultraviolet
VSMOW = Vienna Standard Mean Ocean Water